SIAM J. SCI. COMPUT.
Vol. 26, No. 1, pp. 294–312

BOUNDARY INTEGRAL EVALUATION OF SURFACE DERIVATIVES*

L. J. GRAY†, A.-V. PHAN†‡, AND T. KAPLAN†

Abstract. In boundary element analysis, first order function derivatives, e.g., boundary potential gradient or stress tensor, can be accurately computed by evaluating the hypersingular integral equation for these quantities. However, this approach requires a complete integration over the boundary and is therefore computationally quite expensive. Herein it is shown that this method can be significantly simplified: only *local singular integrals* need to be evaluated. The procedure is based upon defining the singular integrals as a limit to the boundary and exploiting the ability to use both interior and exterior boundary limits. Test calculations for two- and three-dimensional problems demonstrate the accuracy of the method.

Key words. boundary integral method, surface derivatives, hypersingular integrals, boundary limit

AMS subject classifications. 65R20, 45E99

DOI. 10.1137/S1064827502406002

1. Introduction.

One class of applications for which the boundary integral method can be particularly effective is *moving boundary problems*, wherein the task is to simulate the evolution of the domain. The excellent review article [30] contains extensive references on two-dimensional applications in fluids and solids; fluid motion studies in three dimensions have been considered in [11, 25]. In particular, recent breaking wave [18] and interface evolution [44] calculations have employed the gradient evaluation method that is the subject of this paper.

In addition, two somewhat different but related problems are contact analysis [31, 36] and shape optimization [9]. The goal in these analyses is to find the (static) geometry, either the contact region or the optimal shape. Thus, as in a moving boundary problem, the domain will evolve during the course of the nonlinear iteration.

With these problems, an obvious advantage that a boundary-only approach has is that remeshing is easier than when using a volume method. Equally important is that determining the primary quantity of interest, the normal velocity of the surface, generally requires knowing the surface gradient of the primary function, e.g., potential gradient or stress tensor on the surface. Similarly, in contact or shape optimization problems, the algorithm for updating the geometry can depend upon knowledge of the surface stress [1, 36, 48]. Integral equations employ a direct representation of the surface and can work directly with derivatives, as opposed to a numerical differentiation of the initial solution; thus, for equivalent computational effort, a more accurate calculation of surface derivatives should be possible. These derivatives will also be

*Received by the editors April 19, 2002; accepted for publication (in revised form) April 29, 2004; published electronically December 9, 2004. This work was supported by the Applied Mathematical Sciences Research Program of the Office of Mathematical, Information, and Computational Sciences, U.S. Department of Energy, under contract DE-AC05-00OR22725 with UT-Battelle, LLC.

http://www.siam.org/journals/sisc/26-1/40600.html

†Computer Science and Mathematics Division, Oak Ridge National Laboratory, Oak Ridge, TN 37831-6367 (ljg@ornl.gov, tsk@ornl.gov).

‡Current address: Mechanical Engineering Department, University of South Alabama, Mobile, AL 36688-0002 (vphan@jaguar1.usouthal.edu).

referred to here as *tangential derivatives*, as the normal derivative or traction is known from the initial boundary integral solution.

Although tangential derivatives can be expressed as boundary integrals of known quantities [27], direct numerical evaluation is complicated by well-known issues associated with the collocation of hypersingular integrals [20, 39, 40, 41]. Moreover, hypersingular collocation at a corner is especially difficult, though it can be accomplished with special interpolation [52]. A survey of previous collocation algorithms for gradient evaluation, most of which is focused on surface stress, is given in [23, 42, 52]. Recent methods include smoothing techniques [19, 37, 38, 53] and direct collocation methods [10, 52]; a comparison of several gradient procedures is presented in [54].

Unlike collocation, Galerkin approximation effectively handles hypersingular integrals and corners without special techniques [8, 16, 17, 22, 29, 33], and a Galerkin approach for tangential derivative evaluation has been presented in [23]. A more ambitious Galerkin-based technique for computing all derivatives at or near the boundary has also been described in [47]. The algorithm in [23] leads to a system of equations for the gradient everywhere on the boundary. Although it produces accurate results, notably at boundary corners/edges, this approach does have one significant drawback. While the coefficient matrix is quite simple—namely, sparse, symmetric positive definite, and trivial to compute—the evaluation of the right-hand-side vector is computationally quite expensive. It requires a complete Galerkin double integration over the entire boundary. The purpose of this paper is to show that almost all of the effort to compute the right-hand side can be avoided, making the Galerkin approach both accurate and efficient.

The new algorithm is based upon the definition of the hypersingular integral as a limit to the boundary [24] and the ability to effectively compute these limits [22]. By taking the difference of the interior and exterior limit equations, the necessary quadrature is reduced to a few singular integrations. This limit process and the modified Galerkin algorithm are described in the next section, while the subsequent section provides the necessary details concerning the evaluation of the hypersingular integrals. Numerical results providing evidence of the accuracy of the method are presented in section 4. Section 5 briefly discusses the advantages and disadvantages of a collocation implementation of the limit-difference equation, while section 6 considers the implementation of the method for a crack surface.

2. Surface gradient. The discussion below is in the context of the three-dimensional Laplace equation $\nabla^2\phi = 0$, with linear interpolation. It should be clear that the method is applicable in two dimensions and carries over to higher order interpolation [21], but it is not obvious that any equation (i.e., Green's function) can be accommodated. This will depend upon the ability to analytically evaluate the limit and the singular integrals. While it is likely that these processes can be made to work in general, the techniques may need to be tailored to the specific Green's function.

In three dimensions there is not a unique tangent vector, and thus it is convenient to use a fixed coordinate system, computing the gradient

$$\nabla\phi = \left(\frac{\partial\phi}{\partial x}, \frac{\partial\phi}{\partial y}, \frac{\partial\phi}{\partial z}\right) , \tag{2.1}$$

rather than a tangential derivative. Moreover, the gradient components are continuous at corners/edges, and thus it is only necessary to solve for a single value. (However, if tangential derivatives are desired, they can be calculated in the same manner, and with appropriate Galerkin weight functions [14], corners do not present a problem.)

In the following the notation $\partial\phi/\partial\mathbf{E}_k$, $k = 1, 2, 3$, is used to denote the directional derivative with respect to one of the unit coordinate vectors.

The boundary integral equation for the potential $\phi(P)$, in a domain $\mathcal{D}$ having boundary Σ, is

$$\phi(P) + \int_\Sigma \left[\phi(Q) \frac{\partial G}{\partial \mathbf{n}}(P,Q) - G(P,Q) \frac{\partial \phi}{\partial \mathbf{n}}(Q) \right] \mathrm{d}Q = 0 \ . \tag{2.2}$$

Here $\mathbf{n} = \mathbf{n}(Q)$ denotes the unit outward normal on the boundary surface, and as usual the Green's function is

$$G(P,Q) = \frac{1}{4\pi r} \ . \tag{2.3}$$

This equation is valid for $P \in \mathcal{D}$, and for $P \in \Sigma$ it is usually written with a *solid angle* coefficient $c(P)$ multiplying the leading term [4, 6],

$$c(P)\phi(P) + \int_\Sigma \left[\phi(Q) \frac{\partial G}{\partial \mathbf{n}}(P,Q) - G(P,Q) \frac{\partial \phi}{\partial \mathbf{n}}(Q) \right] \mathrm{d}Q = 0 \ . \tag{2.4}$$

and the singular integral involving $\partial G/\partial \mathbf{n}$ interpreted as a Cauchy principal value (CPV) [26]. Herein, however, (2.2) is taken as valid for $P \in \mathcal{D} \cup \Sigma$, with the understanding that for $P \in \Sigma$ this singular integral is defined as a limit, the point P approaching the boundary from the *interior* of the domain [34]. To be completely explicit, write (2.2) as

$$\phi(P) + \lim_{P_I \to P} \int_\Sigma \left[\phi(Q) \frac{\partial G}{\partial \mathbf{n}}(P_I,Q) - G(P_I,Q) \frac{\partial \phi}{\partial \mathbf{n}}(Q) \right] \mathrm{d}Q = 0 \ , \tag{2.5}$$

where $P_I \in \mathcal{D}$. Moreover, approaching the boundary from outside the domain, $P_E \in \mathcal{D}^c$, is equally valid, in which case there is no *free term*,

$$\lim_{P_E \to P} \int_\Sigma \left[\phi(Q) \frac{\partial G}{\partial \mathbf{n}}(P_E,Q) - G(P_E,Q) \frac{\partial \phi}{\partial \mathbf{n}}(Q) \right] \mathrm{d}Q = 0 \ . \tag{2.6}$$

Note that while (2.5) and (2.6) appear to be different, they are in fact precisely the same equation: the jump in the CPV integral as one crosses the boundary accounts for the free term difference. This will *not* be the case for the corresponding tangential derivative equations, and it is this observation that will be exploited in the new algorithm.

From (2.5) a gradient component can be expressed as

$$\frac{\partial \phi(P)}{\partial \mathbf{E}_k} = \lim_{P_I \to P} \int_\Sigma \left[\frac{\partial G}{\partial \mathbf{E}_k}(P_I,Q) \frac{\partial \phi}{\partial \mathbf{n}}(Q) - \phi(Q) \frac{\partial^2 G}{\partial \mathbf{E}_k \partial \mathbf{n}}(P_I,Q) \right] \mathrm{d}Q \ . \tag{2.7}$$

Once the boundary value problem has been solved, all quantities on the right-hand side are known: a direct evaluation of nodal derivatives would therefore be easy were it not for difficulties with the hypersingular integral. As described in [23], a Galerkin approximation of this equation,

$$\begin{aligned} &\int_\Sigma \hat{\psi}_k(P) \frac{\partial \phi(P)}{\partial \mathbf{E}_k} \, \mathrm{d}P \\ &= \lim_{P_I \to P} \int_\Sigma \hat{\psi}_k(P) \int_\Sigma \left[\frac{\partial G}{\partial \mathbf{E}_k}(P_I,Q) \frac{\partial \phi}{\partial \mathbf{n}}(Q) - \phi(Q) \frac{\partial^2 G}{\partial \mathbf{E}_k \partial \mathbf{n}}(P_I,Q) \right] \mathrm{d}Q \, \mathrm{d}P, \end{aligned} \tag{2.8}$$

allows a treatment of the hypersingular integral using standard continuous elements. The weight function $\hat{\psi}_k(P)$ denotes all shape functions which are nonzero at a particular node P_k. Interpolating $\partial\phi(P)/\partial\mathbf{E}_k$ as a linear combination of the shape functions results in a simple system of linear equations for nodal values of the derivative everywhere on Σ; the coefficient matrix is obtained by simply integrating products of two shape functions. Nevertheless, the advantages of this method come at a high price, as the complete boundary integrations required to compute the right-hand side are quite expensive.

The computational cost of this procedure can be significantly reduced by exploiting the exterior limit equation, (2.6). It appears to be useless for computing tangential derivatives for, lacking the free term, the corresponding derivative equation takes the form

$$0 = \lim_{P_E \to P} \int_\Sigma \left[\frac{\partial G}{\partial \mathbf{E}_k}(P_E, Q) \frac{\partial \phi}{\partial \mathbf{n}}(Q) - \phi(Q) \frac{\partial^2 G}{\partial \mathbf{E}_k \partial \mathbf{n}}(P_E, Q) \right] \mathrm{d}Q \ , \tag{2.9}$$

and the derivatives obviously do not appear. However, subtracting this equation from (2.7) yields (with shorthand notation)

$$\frac{\partial \phi(P)}{\partial \mathbf{E}_k} = \left\{ \lim_{P_I \to P} - \lim_{P_E \to P} \right\} \int_\Sigma \left[\frac{\partial G}{\partial \mathbf{E}_k} \frac{\partial \phi}{\partial \mathbf{n}}(Q) - \phi(Q) \frac{\partial^2 G}{\partial \mathbf{E}_k \partial \mathbf{n}} \right] \mathrm{d}Q \ . \tag{2.10}$$

The advantage of this formulation is that now *only the terms that are discontinuous crossing the boundary* contribute to the integral. In the Galerkin implementation of (2.10), the integrations that are nonzero are solely the coincident integral and the hypersingular edge-adjacent integral. All nonsingular (by far the most time consuming) and vertex singular integrals drop out. Moreover, for the integrals that do survive, the integrations simplify in that *higher order* terms from the polynomial shape functions are continuous at the boundary and hence also vanish.

Thus, the calculation of the right-hand side in (2.10) reduces to a few "local" singular integrations. This is intuitively pleasing, as it says that $\partial\phi/\partial\mathbf{E}_k$ at a particular point P is determined entirely by neighboring values of potential and flux (though in the Galerkin approach derivative values are coupled through the linear equations). Note that when $\mathbf{E}_k$ happens to be the normal at a particular point, the hypersingular integral is continuous crossing the boundary; it therefore drops out, appropriately leaving only contributions from the $\partial\phi/\partial\mathbf{n}(Q)$ term. Similarly, if $\mathbf{E}_k$ is a tangent vector, then the $\partial\phi/\partial\mathbf{n}(Q)$ integral will be zero.

Note that subtracting the interior and exterior potential equations, or for that matter, interior and exterior normal derivative equations, would yield no information, simply $0 = 0$. This is not the case for any nonnormal directional derivative: the integrand only contains potential and flux, and thus cancellation of the free term cannot occur. Thus, (2.9) does in fact provide useful information.

Necessary to implementing the Galerkin approximation of (2.10) is the ability to evaluate the limits. Hybrid analytical/numerical limit evaluation algorithms, for the flux (normal derivative) equation, have been described in [22]. However, for a general directional derivative, the analysis of the coincident hypersingular kernel requires an additional step, and this modification will be discussed in the next section.

3. Limit evaluation. The Galerkin form of (2.9) is

$$\int_\Sigma \psi_k(P)\frac{\partial\phi(P)}{\partial\mathbf{E}_k}\,\mathrm{d}P = \left\{\lim_{P_I\to P} - \lim_{P_E\to P}\right\}\int_\Sigma \hat{\psi}_k(P)\int_\Sigma\left[\frac{\partial G}{\partial\mathbf{E}_k}\frac{\partial\phi}{\partial\mathbf{n}}(Q) - \phi(Q)\frac{\partial^2 G}{\partial\mathbf{E}_k\partial\mathbf{n}}\right]\mathrm{d}Q\,\mathrm{d}P\ . \tag{3.1}$$

The most notable difference between this equation and the normal derivative equation relates to the divergences in the integrals. For the flux equation, using either an exterior or interior limit, the coincident and edge-adjacent hypersingular integrals are not separately finite [22]. The divergent terms that arise are of the form $\alpha\log(|\epsilon|)$, ϵ being the distance from the boundary, and it is necessary to prove cancellation of these terms. However, the divergent quantities are in fact independent of the sign of ϵ (i.e., limit direction), and therefore cancel out in (3.1). Thus, the coincident and edge-adjacent hypersingular integrals are independently finite quantities, and in this sense (3.1) is simpler to deal with than the normal derivative equation.

As noted above, the difference of the limits wipes out all contributions except the coincident and adjacent edge singular integrals, and in the latter case, only the hypersingular integral contributes. The singular integration algorithms for implementing these remaining terms are almost entirely the same as presented in [22]. The one key difference is, not surprisingly, with the coincident hypersingular integration. The discussion here will therefore be confined to this integral; complete algorithms can be constructed based upon the details provided in [22]. For simplicity of notation, the $\lim_{P_I\to P} - \lim_{P_E\to P}$ will be omitted, it being understood that the integrals are thus defined.

For this discussion, linear shape functions for a three-noded triangle are employed. Higher order interpolation would add some additional steps to the analysis, but presents no essential difficulty: the general procedure is to split off a singular term that can be integrated analytically (similar to terms from the linear element analysis), plus a nonsingular remainder [21]. For gradient evaluation, the nonsingular terms are continuous crossing the boundary and will therefore disappear in the limit.

The linear shape functions

$$\psi_1(\eta,\xi) = \frac{\sqrt{3}(1-\eta)-\xi}{2\sqrt{3}},\qquad \psi_2(\eta,\xi) = \frac{\sqrt{3}(1+\eta)-\xi}{2\sqrt{3}},\qquad \psi_3(\eta,\xi) = \frac{\xi}{\sqrt{3}} \tag{3.2}$$

are defined on the equilateral parameter space $-1\le\eta\le 1$, $0\le\xi\le\sqrt{3}(1-|\eta|)$, and the potential $\phi(Q)$ is interpolated as

$$\phi(\eta^*,\xi^*) = \sum_{j=1}^{3}\phi(Q_j)\psi_j(\eta^*,\xi^*)\ . \tag{3.3}$$

($\{\eta,\xi\}$ will denote the parameter space for the P integration, $\{\eta^*,\xi^*\}$ for Q.) For a particular element E, the coincident hypersingular integral is

$$\sum_{j=1}^{3}\phi(Q_j)\int_E\psi_k(P)\int_E\psi_j(Q)\frac{\partial^2 G}{\partial\mathbf{E}_k\partial\mathbf{n}}\,\mathrm{d}Q\,\mathrm{d}P\ , \tag{3.4}$$

and the kernel function is given by

$$\frac{\partial^2 G}{\partial\mathbf{E}_k\partial\mathbf{n}}(P,Q) = \frac{1}{4\pi}\left(\frac{\mathbf{n}\bullet\mathbf{E}_k}{r^3} - 3\frac{(\mathbf{n}\bullet\mathbf{R})(\mathbf{E}_k\bullet\mathbf{R})}{r^5}\right)\ . \tag{3.5}$$

Here $\mathbf{R} = Q - (P \pm \epsilon \mathbf{N})$, $r = \|\mathbf{R}\|$ is the distance between Q and the shifted P, and $\mathbf{N}$ is the unit outward normal on the P element. Thus, the plus (resp., minus) sign corresponds to an exterior (resp., interior) limit. The difference between normal and tangential derivative analysis is that for the flux equation, $\mathbf{N} \bullet \mathbf{R}$ is simply $\pm\epsilon$; for tangential, $\mathbf{E}_k \bullet \mathbf{R}$ is obviously the kth component of $\mathbf{R}$.

Transferring to parameter spaces, (3.4) becomes the four-dimensional integral

$$\sum_{j=1}^{3} \phi(Q_j) \int_{-1}^{1} \int_{0}^{\sqrt{3}(1-|\eta|)} \psi_k(\eta,\xi) \int_{-1}^{1} \int_{0}^{\sqrt{3}(1-|\eta^*|)} \psi_j(\eta^*,\xi^*) \frac{J_P^2 \partial^2 G}{\partial \mathbf{E}_k \partial \mathbf{n}} \, \mathrm{d}\xi^* \mathrm{d}\eta^* \, \mathrm{d}\xi \mathrm{d}\eta \ . \tag{3.6}$$

As discussed in [22], evaluation of this integral involves two polar coordinate transformations and analytic integration of the radial variables. The first step is to replace $\{\eta^*, \xi^*\}$ with a polar coordinate system centered at (η, ξ),

$$\begin{aligned} \eta^* - \eta &= \rho \cos(\theta) \ , \\ \xi^* - \xi &= \rho \sin(\theta) \ , \end{aligned} \tag{3.7}$$

and integrate ρ analytically. Note that $0 < \rho < Q_R$ and that writing a formula for $Q_R = Q_R(\eta, \xi, \theta)$ necessitates decomposing the Q parameter space into three subtriangles; as in [22], it suffices to examine the lower subtriangle defined by $\eta^* = 0$. With this transformation,

$$\mathbf{R} = (\, a_1 \rho \pm N_1 \epsilon, a_2 \rho \pm N_2 \epsilon, a_3 \rho \pm N_3 \epsilon \,) \ , \tag{3.8}$$

and thus, independent of limit direction, $r^2 = (a^2 \rho^2 + \epsilon^2)$, with $a^2 = \| \, (a_1, a_2, a_3) \, \|$. It is important to note that the coefficients in $\mathbf{R}$ are of the form

$$a_k = a_k(\theta) = a_{k,c} \cos(\theta) + a_{k,s} \sin(\theta) \, , \tag{3.9}$$

where $a_{k,c}$ and $a_{k,s}$ are functions only of the nodal coordinates of E.

The shape function $\psi_j(Q)$ is a linear function of ρ. However, only the most singular term, namely, $\psi_j(\eta^*, \xi^*)$, evaluated at $\rho = 0$ (equal to $\psi_j(\eta, \xi)$) causes any problem. This is a constant as far as the ρ integration is concerned, and thus this coefficient will be dropped from subsequent formulas. The integrand, the difference of the interior and exterior kernel functions, is then

$$-6 \, \frac{\epsilon \, J_P^2 \, a_k \, \rho}{(\epsilon^2 + a^2 \, \rho^2)^{5/2}} \ , \tag{3.10}$$

and integrating $0 < \rho < Q_R$ yields

$$-2 \, \frac{1}{\epsilon} \, \frac{J_P^2 Q_R^3 \, a_k}{(\, \epsilon^2 + a^2 \, Q_R^2 \,)^{3/2}} \ . \tag{3.11}$$

This quantity behaves as ϵ^{-1} as $\epsilon \to 0$ and is clearly a problem. A term of this form does not show up in the integration of the normal derivative kernel, and thus the treatment of this apparently divergent quantity is the new aspect of the analysis. Fortunately, as will now be shown, this divergence cancels on its own. Note that the limiting form of (3.11), obtained by replacing $(\, \epsilon^2 + a^2 \, Q_R^2 \,)^{-3/2}$ with $a^{-3} \, Q_R^{-3}$, satisfies

$$\int_0^{2\pi} -\frac{2 J_P^2 a_k}{a^3 \epsilon} \, \mathrm{d}\theta = -\frac{2 J_P^2}{\epsilon} \int_0^{2\pi} \frac{a_k}{a^3} \, \mathrm{d}\theta = 0 \ . \tag{3.12}$$

This follows from (3.9), noting that $a_k(\theta+\pi) = -a_k(\theta)$ and $a(\theta+\pi) = a(\theta)$ (in hypersingular integration, divergences cancel out after integrating completely around the singular point [24], and this is the origin of the difficulties with collocation mentioned in the introduction). It is therefore permissible to subtract this limiting quantity from (3.11), resulting in

$$-2\,\frac{1}{\epsilon}\,\frac{J_P^2 a_k\,\left(\,Q_R^3\,a^3 - (\,\epsilon^2 + a^2\,Q_R^2\,)^{3/2}\,\right)}{a^3\,(\,\epsilon^2 + a^2\,Q_R^2\,)^{3/2}}\ . \tag{3.13}$$

The Taylor series expansion of the numerator is a function of ϵ^2, and would seem to indicate that this quantity vanishes in the limit. However, during the course of the P integration, P will come close to the element edges, in which case Q_R also becomes small. Thus, the Taylor expansion is not applicable, and (3.13) is not a viable form for examining the limit $\epsilon \to 0$. Nevertheless, progress has been made, and it is clear that this quantity is less singular at $\epsilon = 0$ than its predecessor (3.11).

As discussed in [22], the necessary second analytic integration proceeds by first replacing θ with t,

$$\theta = -\frac{\pi}{2} + \tan^{-1}\left(\frac{t-\eta}{\xi}\right)\ , \tag{3.14}$$

and then employing a second polar coordinate transformation $\{\Lambda, \Psi\}$,

$$\begin{aligned} t &= \Lambda\cos(\Psi) + \eta\ , \\ \xi &= \Lambda\sin(\Psi)\ . \end{aligned} \tag{3.15}$$

Analytic integration with respect to Λ of (3.13), and then letting $\epsilon \to 0$, finally yields

$$\frac{4 J_P^2 a_k \sin(\Psi)}{a^4}\ . \tag{3.16}$$

(This is the result for the lowest order term in Λ; higher order terms follow similarly.) This quantity is perfectly well behaved as a function of the remaining variables η and Ψ, and can be integrated numerically. Thus, it is important to note that even though there are no $\log(\epsilon)$ divergences in the coincident integral, the limit process is effective in (exactly) removing potentially divergent quantities that could cause numerical problems.

4. Test calculations. For the test examples, symmetric-Galerkin approximation, based upon linear triangular elements described above, is employed to solve several initial boundary value problems. These solutions are then used to compute the surface gradient.

The first test is a simple mixed boundary value problem inside the unit square $0 < \{\,x, y, z\,\} < 1$. The boundary conditions are $\phi(x, y, z) = x$ on $x = 0$ and $x = 1$, and zero flux elsewhere, and thus the exact solution is $\phi(x, y, z) = x$, $\partial\phi/\partial y = \partial\phi/\partial z = 0$, and $\partial\phi/\partial x = 1$. A crude discretization having 48 uniform elements and 56 nodes is employed. The purpose of this example is primarily to check that the adjacent edge contributions are correctly handled at boundary edges and corners. The computed normal derivative and gradient at the cube corners are listed in Table 1. Note that the errors in the gradient are no worse than in the computed normal derivative.

The second test problem has prescribed potential $\phi(x, y, z) = x$ for the (interior) unit sphere, discretized using 896 nonuniform linear triangular elements, comprising

TABLE 1
Computed normal derivative and gradient at the corners of the unit cube.

Point	$\phi_{,n}$	$\phi_{,x}$	$\phi_{,y}$	$\phi_{,z}$
$(0,0,0)$	-1.02372	1.00488	-0.00181	-0.00181
$(0,1,0)$	-1.00617	1.00210	0.00113	-0.00127
$(0,1,1)$	-1.02418	1.00379	0.00187	0.00187
$(0,0,1)$	-1.00617	1.00210	0.00127	-0.00113
$(1,0,0)$	0.97234	0.98426	0.00192	0.00192
$(1,1,0)$	1.00122	0.99667	-0.00111	0.00121
$(1,1,1)$	0.97355	0.99035	-0.00104	-0.00104
$(1,0,1)$	1.00122	0.99667	0.00121	0.00111

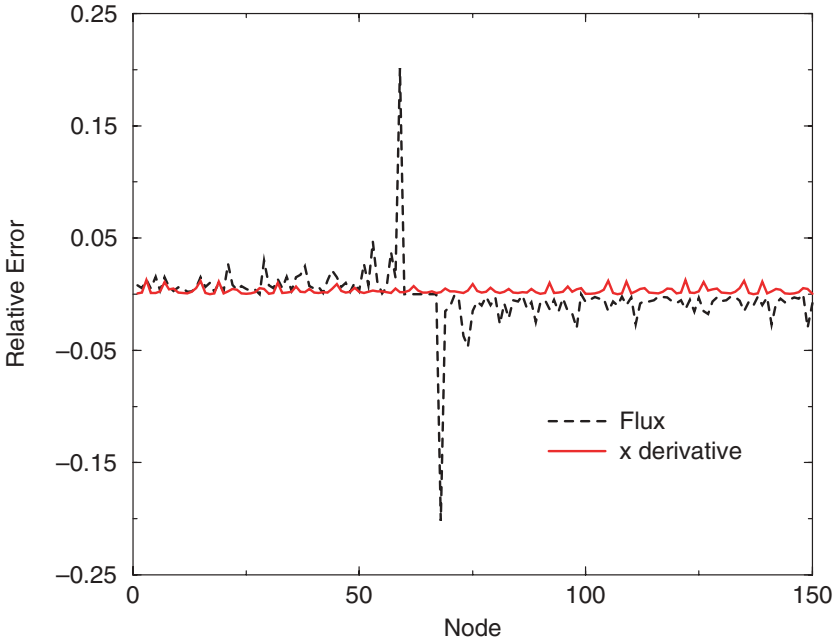

FIG. 1. *Relative error in the flux solution and the x-component of the surface gradient for the interior Dirichlet problem on the unit sphere.*

450 nodes. The gradient on the boundary is therefore $(1,0,0)$, and since $\mathbf{n} = (x,y,z)$, the computed flux should also be $\partial\phi/\partial\mathbf{n} = x$. As these functions are linear, the only errors come from the linear approximation of the spherical surface and the numerical quadratures, and thus accurate answers are expected. Figure 1 displays the relative error in the computed flux, together with the error (absolute and relative being the same in this case) in the x-component of the gradient (for clarity, only the first 150 nodes are shown; the remainder of the curves look quite similar). The spikes in the flux error correspond to nodes for which the exact solution is small; the absolute errors at these nodes are comparable to the rest of the sphere. This is born out by the accurate results for $\partial\phi/\partial x$. As the remaining components of the gradient should be zero, Figure 2 plots the absolute error in the y- and z-components. These figures show that, roughly speaking, the gradient is computed with the same level of accuracy as the flux, which is the best that can be hoped for.

Note that in this example the potential is known exactly, and thus no error is

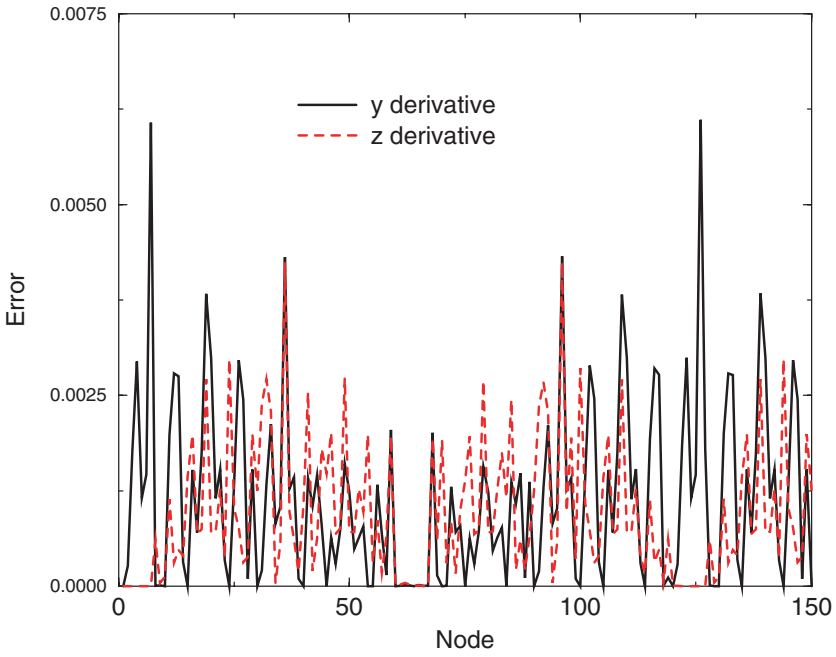

FIG. 2. *Absolute error in the y- and z-components of the surface gradient.*

introduced into the hypersingular integral from the coefficient function. To test what happens for the reverse situation, consider a Neumann problem posed on the exterior of the unit sphere. The exact solution sought is

$$\phi(x,y,z) = \frac{x}{(x^2+y^2+z^2)^{3/2}} \ , \tag{4.1}$$

and thus the surface gradient is

$$\nabla\phi(x,y,z) = \left(1-3x^2, -3xy, -3xz\right), \tag{4.2}$$

applied surface flux ($\mathbf{n} = -(x,y,z)$) is

$$\frac{\partial\phi}{\partial\mathbf{n}}(x,y,z) = 2x \ . \tag{4.3}$$

Note that the gradient is a quadratic function, and consequently larger errors (due to the linear interpolation) should result. Figure 3 displays the relative error in the computed gradient. Again, the spikes correspond to regions for which the exact solution is small. This is corroborated by Figure 4, which plots the absolute error in the initial potential solution and in the x-component of the gradient (the worst offender in Figure 3). The larger errors in the gradient are due to the fact that the exact solution in this case is a quadratic, and thus the linear approximation should introduce more error.

Finally, a simple two-dimensional calculation is considered, an interior Dirichlet problem on the unit disk. The boundary condition is $\phi(x,y) = x^2 - y^2$, and the solution for the surface flux is obtained using a linear element Galerkin method. The postprocessing of the surface gradient is again computed using linear interpolation.

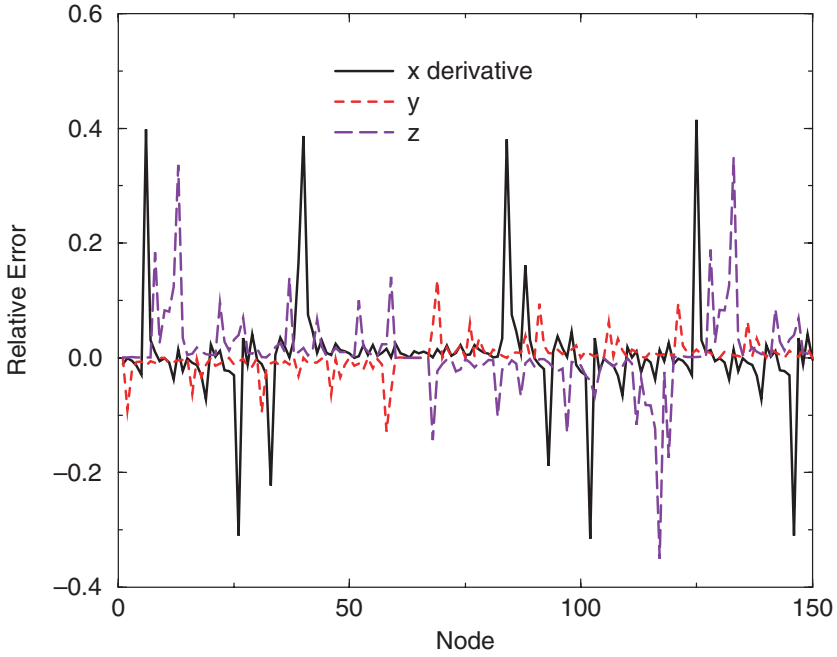

FIG. 3. *Relative error in the gradient components for the exterior Neumann problem.*

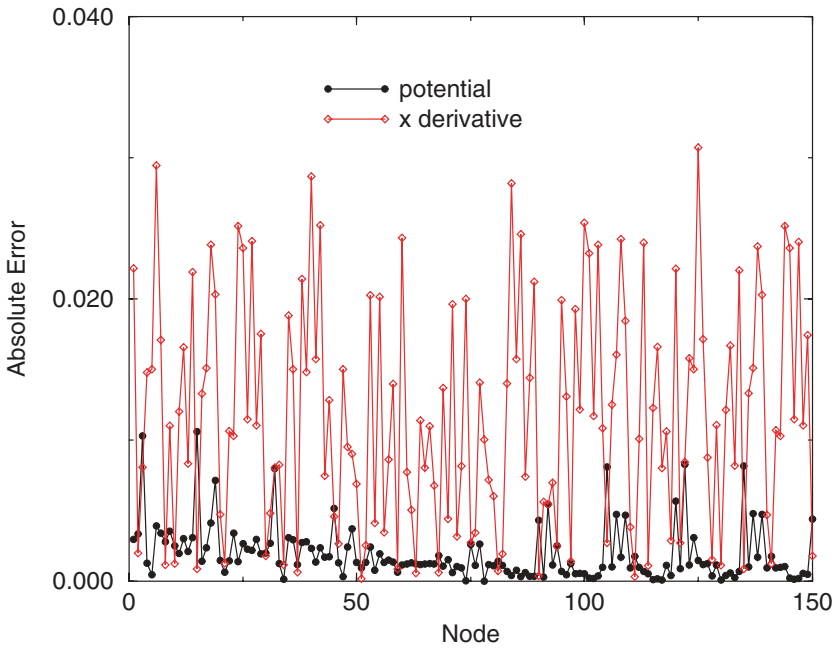

FIG. 4. *Absolute error in the computed potential and the x-component of the gradient.*

TABLE 2
L^2 errors for the gradient for the two-dimensional problem on the unit disk.

Elements	L^2 error
25	0.1731E−1
50	0.4207E−2
100	0.1044E−2
150	0.4632E−3
200	0.2604E−3
250	0.1666E−3
300	0.1157E−3
350	0.8498E−4
400	0.6506E−4

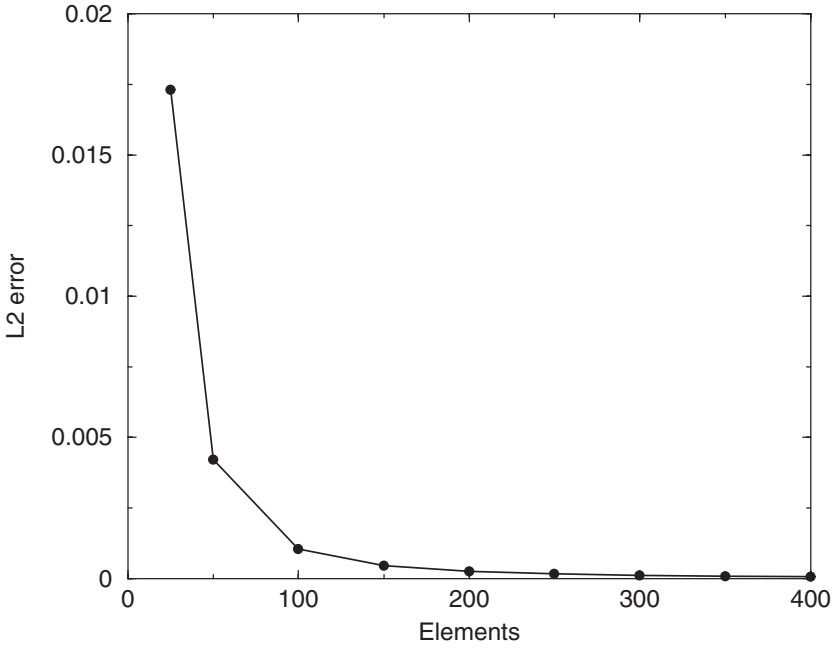

FIG. 5. *Convergence of the computed gradient for the Dirichlet problem on the unit disk.*

Table 2 lists the L^2 errors in the x-component of the gradient (the y-component is similar) for various uniform discretizations of the unit circle, and these data are plotted in Figure 5. It can be seen that the convergence obtained with linear interpolation is approximately quadratic.

5. Collocation. In section 3, it was demonstrated that, by taking the difference of the interior and exterior limits, the divergences present in the coincident and edge-adjacent integrals vanish. One might then ask if the $\log(\epsilon)$ terms that arise from *collocating* the interior limit equation, (2.7), will also disappear in (2.10). If this were to happen, the difficult C^1 interpolation constraint discussed in the introduction would no longer apply, and a simple gradient collocation algorithm could be constructed. Note that the important advantage of this approach would be that individual nodal gradients could be computed; i.e., there is no system of equations to solve. In this section it is shown that the $\log(\epsilon)$ contributions do indeed self-cancel in collocating (2.10). However, analogous to (3.11), a $1/\epsilon$ singularity remains, and disposing of this

term, as in (3.12) for Galerkin, is not as easy. Thus, while collocation may be useful, there are aspects of this algorithm that are less than satisfactory.

As in the Galerkin formulation, all nonsingular integrals in (2.7) vanish, and thus to obtain the gradient at a particular node P_0, only those elements containing P_0 need be considered. It also suffices to examine the hypersingular kernel; the integral involving the first derivative of G is handled similarly and moreover causes no problems. Thus, the following discussion considers the evaluation of

$$\left\{ -\lim_{P_I \to P_0} - \lim_{P_E \to P_0} \right\} \int_\Sigma \phi(Q) \frac{\partial^2 G}{\partial \mathbf{E}_k \partial \mathbf{n}}(P_{\{I,E\}}, Q)\, \mathrm{d}Q \ . \tag{5.1}$$

Note that there must be a fixed limit direction for P_0, and thus it cannot be assumed that the approach is normal to the element. Even if the surface is smooth, the linear element interpolation will produce a faceted approximation. Thus, a general direction (unit vector) $\mathbf{L} = (L_1, L_2, L_3)$ is assumed; one possible algorithm for choosing L is to average the normals of the elements containing P_0.

To evaluate the integral, assume that P_0 corresponds to the point $\eta^* = -1$, $\xi^* = 0$ in the equilateral parameter space, and introduce polar coordinates

$$\begin{aligned} \eta^* &= \rho \cos(\theta) - 1 \ , \\ \xi^* &= \rho \sin(\theta) \ , \end{aligned} \tag{5.2}$$

where $0 \le \rho \le Q_R = \sqrt{3}/(\sqrt{3}\cos(\theta) + \sin(\theta))$ and $0 \le \theta \le \pi/3$. As before, ρ will be integrated analytically, and θ numerically. As in (3.8),

$$\mathbf{R} = (\, a_1\rho \pm L_1\epsilon, a_2\rho \pm L_2\epsilon, a_3\rho \pm L_3\epsilon \,) \,, \tag{5.3}$$

but now

$$r^2 = (a^2\rho^2 \pm b_1\epsilon\rho + \epsilon^2) \ . \tag{5.4}$$

Note that the shape functions (3.2) become

$$\begin{aligned} \psi_1(\eta^*, \xi^*) &= 1 - \frac{1}{2\sqrt{3}}\rho \left(\sqrt{3}\cos(\theta) + \sin(\theta) \right) , \\ \psi_2(\eta^*, \xi^*) &= \frac{1}{2\sqrt{3}}\rho \left(\sqrt{3}\cos(\theta) - \sin(\theta) \right) , \\ \psi_3(\eta^*, \xi^*) &= \rho \frac{\sin(\theta)}{\sqrt{3}} \ . \end{aligned} \tag{5.5}$$

Thus, dropping the interior/exterior limits once again, the two integrals to consider are

$$-j_q \int_0^{\pi/3} \int_0^{Q_R} \rho^k \frac{\partial^2 G}{\partial \mathbf{E}_k \partial \mathbf{n}}(P, Q)\, \mathrm{d}\rho\, \mathrm{d}\theta \ , \tag{5.6}$$

where j_q is the Jacobian and $k = 1, 2$; the extra factor of ρ comes from the polar transformation. For the interior limit alone, the $k = 2$ integral is responsible for producing the $\log(\epsilon)$ term. However, in the difference of the limits the divergent term drops out of the ρ integration, leaving

$$-\frac{4j_q}{a^2} \left(\frac{8a^2 \mathbf{n} \bullet \mathbf{L}(2a_k + L_k b_1)}{(4a^2 - b_1^2)^2} - \frac{\mathbf{n}_k b_1}{(4a^2 - b_1^2)} \right) \tag{5.7}$$

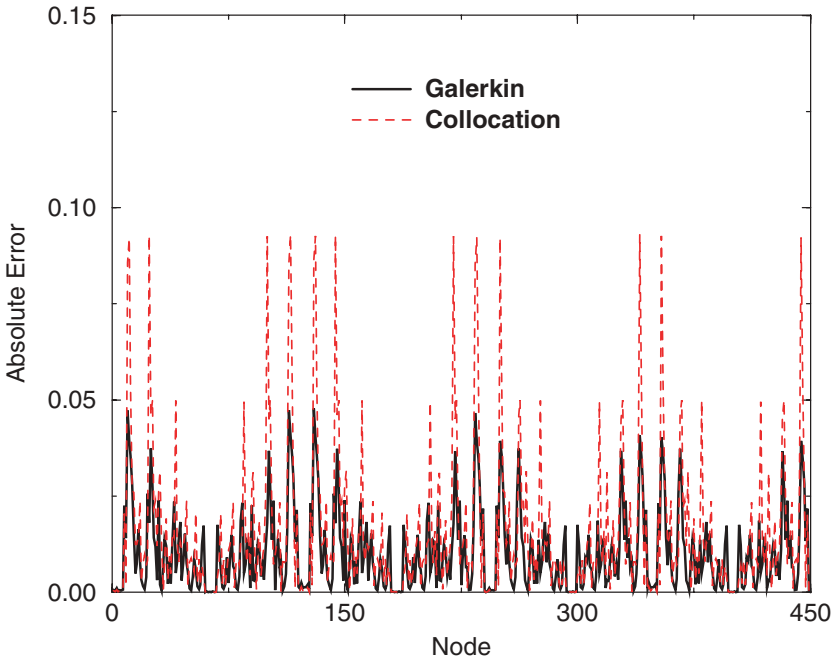

FIG. 6. *The absolute errors, Galerkin and collocation, in the z-component of the gradient.*

to be integrated with respect to θ. Thus, there is no C^1 interpolation constraint for $\phi(Q)$. For $k = 0$, however, we find

$$-\frac{1}{\epsilon}\frac{4j_q}{a(4a^2-b_1^2)^2}\left(\mathbf{n}\bullet\mathbf{L}(8a^2a_k+2a_kb_1^2+8a^2L_kb_1)-\mathbf{n}_ka_1(4a^2-b_1^2)\right), \tag{5.8}$$

which is clearly a problem at $\epsilon = 0$. *If*, instead of the faceted approximation that results from standard C^0 elements, the surface were C^1, then the coefficients $\{a_k\}$ would have one value over the complete neighborhood of P_0, and this term would integrate to zero for precisely the same reason as (3.12). However, interpolating and integrating each element individually, there is a different set of $\{a_k\}$ for each element. Thus, with standard (faceted surface) boundary integral approximations, it is not at all clear that cancellation will occur. The limit-difference therefore removes the C^1 condition on ϕ, but not on the boundary interpolation.

For Laplace (and elasticity) this difficulty can be side-stepped by noting that a constant function satisfies the differential equation, and that shifting by a constant is immaterial as far as the gradient calculation is concerned. From (5.5), the problematic $k = 0$ integral only multiplies $\phi(P_0)$, and thus replacing $\phi(Q)$ by $\phi(Q) - \phi(P_0)$ will effectively kill off the $1/\epsilon$ divergent term.

To test the algorithm, the exterior Neumann sphere problem solved by means of the Galerkin algorithm has been investigated using the collocation method. Figure 6 plots the absolute error for the two approaches for the z-component of the gradient (the remaining two are similar). The L^2 error for Galerkin is 0.6910×10^{-3} and 0.1177×10^{-2} for collocation. Thus, while the collocation algorithm is successful, it is less accurate than the Galerkin method. The Galerkin method is of course more expensive, but in general for moving boundary applications, one would prefer to pay the price and get a more accurate result for the critical surface velocity.

This collocation gradient algorithm therefore has two major drawbacks. It is less accurate than Galerkin, and it does not appear to be applicable if a constant function is not a solution of the differential equation (e.g., Helmholtz equation). In addition, the trick of shifting the potential will not work on a crack surface. As will be discussed in the next section, the variable is the jump in potential across the crack, and thus subtracting a constant from the potential accomplishes nothing. However, one useful role for this method might be for truncating Galerkin equations. In many applications, the gradient is only needed on a part of the boundary, and thus the ability to truncate the Galerkin system of equations to a region of interest would be very useful. This procedure might go as follows: somewhat outside and surrounding the region of interest, use the collocation equations to compute individual gradient values. As these quantities are not of interest for the subsequent analysis, the errors resulting from ignoring the C^1 interpolation constraint (and collocation method) should not be a problem. When these somewhat inaccurate values can be used to terminate the Galerkin equations, the errors should have little effect. An alternative to this collocation termination is to use one of the "local" methods discussed in the literature [13, 45, 51].

6. Cracks. It is often the case for boundary integral methods that a fracture geometry requires special consideration, and the gradient algorithm is no exception. Although the method is essentially the same as for a noncrack surface, it is not immediately clear how to justify the interior/exterior limit process on a fracture. In this section, the appropriate tangential derivative procedure is described and results of a test calculation are presented. One example where the ability to calculate gradients on a crack is useful is rock mechanics [3, 35].

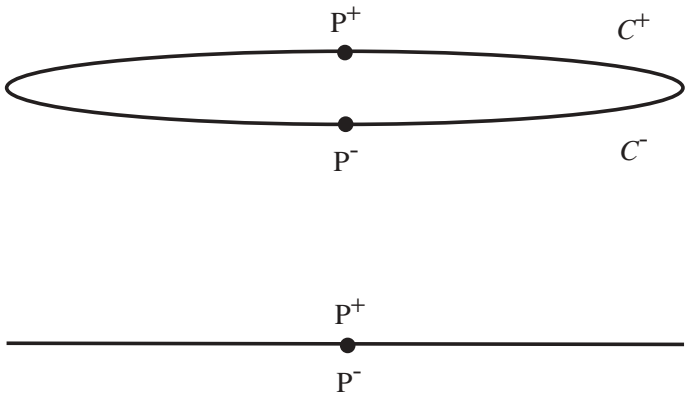

FIG. 7. *Schematic view of a crack as the limiting case of a thin inclusion.*

As shown in Figure 7, a crack can be thought of as the limit of a *thin ellipsoidal* inclusion where the thickness goes to zero; i.e., the opposing faces of the inclusion C^+ and C^- merge and become the same surface. In a displacement discontinuity [12, 49] or symmetric-Galerkin [5, 7, 33, 50] approximation, the fracture is treated as *a single surface*, the appropriate variables being the jump in potential and the sum of the fluxes:

$$[\phi] = \phi(P^+) - \phi(P^-) \ , \tag{6.1}$$

$$\left[\frac{\partial\phi}{\partial\mathbf{n}}\right] = \frac{\partial\phi}{\partial\mathbf{n}}(P^+) + \frac{\partial\phi}{\partial\mathbf{n}}(P^-) \ .$$

Here P^+ and P^- represent the corresponding points on C^+ and C^-. In the initial boundary integral solution, the normal derivative equation is employed on the crack surface. It is worth noting that there is a problem with this equation at the crack front: an element having an edge along the front is missing an adjacent element, which, as discussed above, is necessary to insure that the hypersingular integral is finite. However, this affects only nodes on the crack front, and for these nodes $[\phi] = 0$. Thus, fortunately, no equations are written for these nodes.

Analogously to (6.1), the sum of the gradients across the crack

$$\left[\frac{\partial\phi}{\partial\mathbf{E}_k}\right] = \frac{\partial\phi}{\partial\mathbf{E}_k}(P^+) + \frac{\partial\phi}{\partial\mathbf{E}_k}(P^-) \tag{6.2}$$

is sought. However, as is well known, near the crack front the potential along the surface behaves as $\sqrt{r_f}$, r_f being the distance to the front. Thus, the tangential derivatives will not exist at $r_f = 0$. In the calculation presented below, we simply allow the algorithm to try to compute the nonexistent derivatives, recognizing that this will produce significant errors near the front. Accurate results should nevertheless be obtainable near the center of the crack.

To derive an appropriate gradient algorithm, it is convenient to go back to Figure 7 and view the fracture as having a nonzero thickness. The algorithm described above therefore applies: for a point (say on C^+), only the local singular integrals contribute, e.g., C^- does not enter into the calculation. By not allowing the Galerkin weight functions at the crack front to straddle the front, the gradient equations on C^+ and C^- can be written independently, these equations involving the potential and flux on their respective surfaces. Moreover, the Galerkin coefficient matrix depends solely upon the shape functions, and thus this matrix is the same for both sides of the crack. The C^+ and C^- equations can therefore be combined to produce an equation for sum of gradients across the crack. Not surprisingly, this equation is precisely the result that would be obtained by treating the crack as a single surface, using the *jump* variables in (6.1) instead of ϕ and $\partial\phi/\partial\mathbf{n}$, and then applying the noncrack algorithm.

Although the above discussion has tacitly assumed an embedded crack, an edge crack can be handled in precisely the same fashion. At the junction between a crack and an outer boundary, simply define the Galerkin weight functions so that they do not span both the crack and the outer boundary. As far as the gradient equations are concerned, the crack then appears to be an embedded crack.

As a simple test, consider the "penny-shaped crack" $x^2+y^2 \le R_0 = \sqrt{2}/10$, $z = 0$, in an infinite medium, with boundary condition $[\,\partial\phi/\partial\mathbf{n}\,] = 1$. This "pressurized crack" has the exact solution [32, p. 144]

$$[\phi] = \frac{2R_0}{\pi}\left(1 - \frac{r^2}{R_0^2}\right)^{1/2} \ , \tag{6.3}$$

where $r^2 = x^2 + y^2$. The discretization employed 214 nodes and 382 elements. More importantly, a special crack tip element [2, 43, 28] to capture the $\sqrt{r_f}$ behavior has *not* been employed, and thus some error near the front is expected. Figure 8 compares the exact potential in (6.3) with the computed solution, and while the inappropriate linear element at the front causes some error, this initial solution is generally quite accurate.

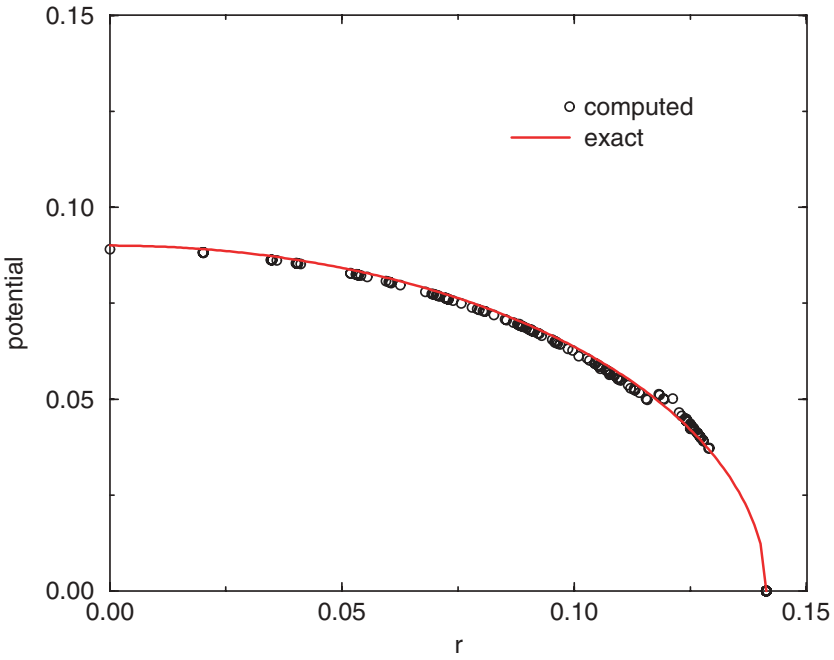

FIG. 8. *The solution for* $[\phi]$ *for the pressurized penny-shaped crack.*

The z-component of the gradient is in this case just the applied boundary condition, and thus for this component there is no singularity at the front. The gradient algorithm returned accurate values, the maximum absolute error being 0.0014. This is not surprising: there are no divergences in either the coincident or adjacent edge integrals, and thus as long as the quantity being computed is finite, valid equations can be written at the crack front. To examine the $\{x, y\}$-components, Figure 9 plots the exact solution for the gradient length (ignoring the z-component)

$$\left(\left[\frac{\partial \phi}{\partial x} \right]^2 + \left[\frac{\partial \phi}{\partial y} \right]^2 \right)^{(1/2)} = \frac{2}{\pi R_0} \frac{r}{1 - r^2/R_0^2} \,. \tag{6.4}$$

As expected, the solution is quite good near the center of the crack and deteriorates as the crack front is approached: without special approximations, the method would not be able to compute a singular function. The oscillation above and below the exact curve is typical behavior when confronting a divergent solution.

7. Conclusions. Galerkin postprocessing evaluation of tangential derivatives is now both accurate *and* efficient. This method should be highly useful for moving boundary problems, as the surface velocity is usually a function of these derivatives. The key to the efficiency is to rewrite the derivative equation as a difference of interior and exterior limits, as it is then only necessary to compute the few integrals that are discontinuous crossing the boundary. This modified Galerkin algorithm obviously retains the other advantages of its predecessor, namely, that *nodal* derivative values are obtained directly, the hypersingular evaluation is accomplished with standard C^0 boundary interpolations, and accurate results are obtained at boundary corners and edges.

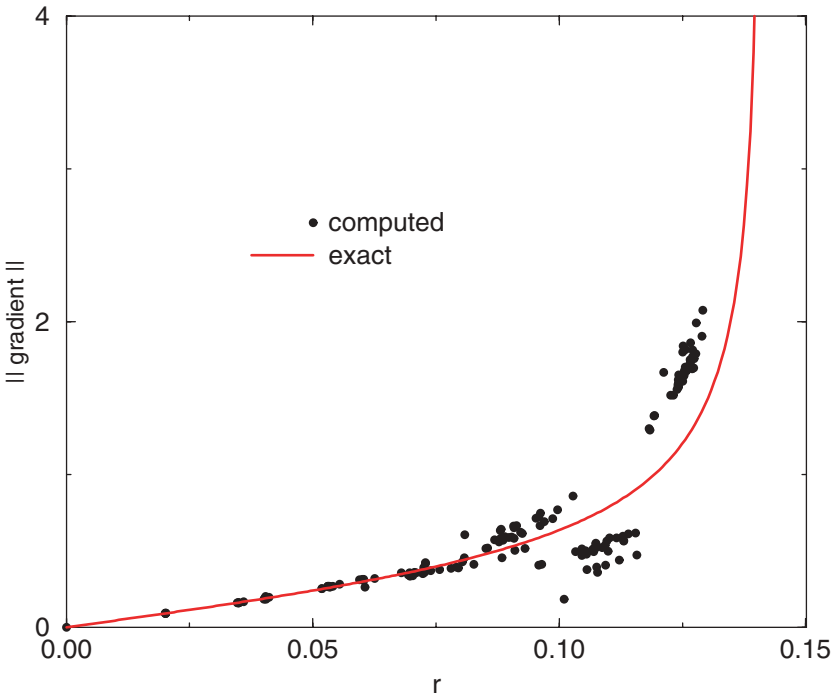

FIG. 9. *A comparison of the exact and computed values for the length of the gradient for the pressurized penny-shaped crack.*

A boundary limit definition of the singular and hypersingular integrals is essential for this new algorithm. This is therefore one application where other techniques for hypersingular evaluation, e.g., Stokes' theorem [16, 33], Hadamard finite part [46], or Duffy transformations [15], are simply not available.

A corresponding collocation algorithm for evaluating the limit-difference equation was found to be less accurate than Galerkin and, moreover, apparently not generally applicable. It could possibly prove useful as a means of truncating the Galerkin equations to a region of interest.

Acknowledgment. The authors would like to thank R. E. Flanery for help in preparing the figures.

REFERENCES

[1] M. R. BARONE, *Boundary integral equations for recovery of design sensitivities in shape optimization*, AIAA J., 26 (1988), pp. 589–594.
[2] R. S. BARSOUM, *On the use of isoparametric finite elements in linear fracture mechanics*, Internat. J. Numer. Methods Engrg., 10 (1976), pp. 25–37.
[3] A. BOBET AND H. H. EINSTEIN, *Numerical modelling of fracture coalescence in a model rock material*, Int. J. Fracture, 92 (1998), pp. 221–252.
[4] M. BONNET, *Boundary Integral Equation Methods for Solids and Fluids*, Wiley and Sons, Chichester, UK, 1995.
[5] M. BONNET, G. MAIER, AND C. POLIZZOTTO, *Symmetric Galerkin boundary element method*, ASME Appl. Mech. Rev., 51 (1998), pp. 669–704.
[6] C. A. BREBBIA, J. C. F. TELLES, AND L. C. WROBEL, *Boundary Element Techniques*, Springer-Verlag, Berlin, New York, 1984.

[7] H. D. Bui, B. Loret, and M. Bonnet, *Régularisation des équations intégrales de l'élastostatique et de l'élastodinamique*, C. R. Acad. Sci. Paris Sér. II Méc. Phys. Chim. Sci. Univers Sci. Terre, 300 (1985), pp. 633–636.
[8] A. Carini, M. Diligenti, P. Maranesi, and M. Zanella, *Analytical integrations for two dimensional elastic analysis by the symmetric Galerkin boundary element method*, Comput. Mech., 23 (1999), pp. 308–323.
[9] A. Chandra and S. Mukherjee, *Boundary Element Methods in Manufacturing*, Oxford University Press, New York, 1997.
[10] M. K. Chati and S. Mukherjee, *Evaluation of gradients on the boundary using fully regularized hypersingular boundary integral equations*, Acta Mech., 135 (1999), pp. 41–45.
[11] J. K. Choi and S. A. Kinnas, *Numerical water tunnel in two- and three-dimensions*, J. Ship Research, 42 (1998), pp. 86–98.
[12] S. L. Crouch, *Solution of plane elasticity problems by the displacement discontinuity method*, Internat. J. Numer. Methods Engrg., 10 (1976), pp. 301–343.
[13] T. A. Cruse and W. Van Buren, *Three-dimensional elastic stress analysis of a fracture specimen with an edge crack*, Internat. J. Fracture Mech., 7 (1971), pp. 1–15.
[14] F. A. de Paula and J. C. F. Telles, *A comparison between point collocation and Galerkin for stiffness matrices obtained by boundary elements*, Engrg. Anal. Boundary Elements, 6 (1989), pp. 123–128.
[15] M. G. Duffy, *Quadrature over a pyramid or cube of integrands with a singularity at a vertex*, SIAM J. Numer. Anal., 19 (1982), pp. 1260–1262.
[16] A. Frangi, *Regularization of boundary element formulations by the derivative transfer method*, in Singular Integrals in the Boundary Element Method, V. Sladek and J. Sladek, eds., Advances in Boundary Elements, Computational Mechanics Publishers, Southampton, UK, 1998, pp. 125–164.
[17] A. Frangi and G. Novati, *Symmetric BE method in two-dimensional elasticity: Evaluation of double integrals for curved elements*, Comput. Mech., 19 (1996), pp. 58–68.
[18] M. Garzon, D. Adalsteinsson, L. J. Gray, and J. A. Sethian, *Wave breaking over sloping beaches using a coupled boundary integral-level set method*, Interfaces Free Boundaries, submitted.
[19] E. Graciani, V. Mantič, F. Paris, and J. Cañas, *A critical study of hypersingular and strongly singular boundary integral representations of potential gradient*, Comp. Mech., 25 (2000), pp. 542–559.
[20] L. J. Gray, *Evaluation of hypersingular integrals in the boundary element method*, Math. Comput. Modelling, 15 (1991), pp. 165–174.
[21] L. J. Gray, *Evaluation of singular and hypersingular Galerkin boundary integrals: Direct limits and symbolic computation*, in Singular Integrals in the Boundary Element Method, V. Sladek and J. Sladek, eds., Advances in Boundary Elements, Computational Mechanics Publishers, Southampton, UK, 1998, pp. 33–84.
[22] L. J. Gray, J. M. Glaeser, and T. Kaplan, *Direct evaluation of hypersingular Galerkin surface integrals*, SIAM J. Sci. Comput., 25 (2004), pp. 1534–1556.
[23] L. J. Gray, D. Maroudas, and M. Enmark, *Galerkin boundary integral method for evaluating surface derivatives*, Comput. Mech., 22 (1998), pp. 187–193.
[24] L. J. Gray, L. F. Martha, and A. R. Ingraffea, *Hypersingular integrals in boundary element fracture analysis*, Internat. J. Numer. Methods Engrg., 29 (1990), pp. 1135–1158.
[25] S. T. Grilli, P. Guyenne, and F. Dias, *A fully nonlinear model for three-dimensional overturning waves over arbitrary bottom*, Internat. J. Numer. Methods Fluids, 35 (2001), pp. 829–867.
[26] M. Guiggiani, *The evaluation of Cauchy principal value integrals in the boundary element method—a review*, Math. Comput. Modelling, 15 (1991), pp. 175–184.
[27] M. Guiggiani, *Hypersingular formulation for boundary stress evaluation*, Engrg. Anal. Boundary Elements, 13 (1994), pp. 169–179.
[28] R. D. Henshell and K. G. Shaw, *Crack tip finite elements are unnecessary*, Internat. J. Numer. Methods Engrg., 9 (1975), pp. 495–507.
[29] S. M. Hölzer, *How to deal with hypersingular integrals in the symmetric BEM*, Comm. Numer. Methods Engrg., 9 (1993), pp. 219–232.
[30] T. Y. Hou, J. S. Lowngrub, and M. J. Shelley, *Boundary integral methods for multicomponent fluids and multiphase materials*, J. Comput. Phys., 169 (2001), pp. 302–362.
[31] K. L. Johnson, *Contact Mechanics*, Cambridge University Press, Cambridge, UK, 1985.
[32] H. Lamb, *Hydrodynamics*, 6th ed., Dover, New York, 1945.
[33] S. Li, M. E. Mear, and L. Xiao, *Symmetric weak form integral equation method for three-dimensional fracture analysis*, Comput. Methods Appl. Mech. Engrg., 151 (1998), pp. 435–459.

[34] E. D. Lutz and L. J. Gray, *Exact evaluation of singular boundary integrals without CPV*, Comm. Numer. Methods Engrg., 9 (1993), pp. 909–915.
[35] L. Maerten, E. J. M. Willemse, D. D. Pollar, and K. Rawnsley, *Slip distributions on intersecting normal faults*, J. Structural Geology, 21 (1999), pp. 259–271.
[36] S. Maiti, G. H. Paulino, and P. H. Geubelle, *A novel frictionless contact formulation and implementation using the boundary element method*, Internat. J. Numer. Methods Engrg., to appear.
[37] V. Mantič, E. Graciani, and F. Paris, *Potential gradient recovery using a local smoothing procedure in the Cauchy integral*, Comm. Numer. Methods Engrg., 15 (1999), pp. 547–556.
[38] V. Mantič, E. Graciani, and F. Paris, *A simple local smoothing scheme in strongly singular boundary integral representation of potential gradient*, Comput. Methods Appl. Mech. Engrg., 178 (1999), pp. 267–289.
[39] P. A. Martin and F. J. Rizzo, *On boundary integral equations for crack problems*, Proc. Roy. Soc. London Ser. A, 421 (1989), pp. 341–355.
[40] P. A. Martin and F. J. Rizzo, *Hypersingular integrals: How smooth must the density be?*, Internat. J. Numer. Methods Engrg., 39 (1996), pp. 687–704.
[41] P. A. Martin, F. J. Rizzo, and T. A. Cruse, *Smoothness-relaxation strategies for singular and hypersingular integral equations*, Internat. J. Numer. Methods Engrg., 42 (1998), pp. 885–906.
[42] T. Matsumoto, M. Tanaka, and H. Hirata, *Boundary stress calculation using regularized boundary integral equation for displacement gradients*, Internat. J. Numer. Methods Engrg., 36 (1993), pp. 783–797.
[43] A.-V. Phan, L. J. Gray, G. H. Paulino, and T. Kaplan, *Improved quarter-point crack tip element*, Engrg. Fracture Mech., 70 (2003), pp. 269–283.
[44] A.-V. Phan, T. Kaplan, L. J. Gray, D. Adelsteinsson, J. A. Sethian, W. Barvosa-Carter, and M. A. Aziz, *Modeling a growth instability in a stressed solid*, Modelling Simul. Mater. Sci. Engrg., 9 (2001), pp. 309–325.
[45] F. J. Rizzo and D. J. Shippy, *A formulation and solution procedure for the general nonhomogeneous elastic inclusion problem*, Internat. J. Solids Struct., 4 (1968), pp. 1161–1173.
[46] A. Salvadori, *Analytical integrations of hypersingular kernel in* 3D *BEM problems*, Comput. Methods Appl. Mech. Engrg., 190 (2001), pp. 3957–3975.
[47] C. Schwab and W. L. Wendland, *On the extraction technique in boundary integral equations*, Math. Comp., 68 (1999), pp. 91–122.
[48] J. A. Sethian and A. Wiegmann, *Structural boundary design via level set and immersed interface methods*, J. Comput. Phys., 163 (2000), pp. 489–528.
[49] E. Siebritz and S. L. Crouch, *Two-dimensional elastodynamic displacement discontinuity method*, Internat. J. Numer. Methods Engrg., 37 (1994), pp. 3229–3250.
[50] S. Sirtori, *General stress analysis method by means of integral equations and boundary elements*, Meccanica, 14 (1979), pp. 210–218.
[51] V. Sladek and J. Sladek, *Improved computation of stresses using the boundary element method*, Appl. Math. Modelling, 10 (1986), pp. 249–255.
[52] A. J. Wilde and M. H. Aliabadi, *Direct evaluation of boundary stresses in the* 3*D BEM of elastostatics*, Comm. Numer. Methods Engrg., 14 (1998), pp. 505–517.
[53] Z. Y. Zhao, *Interelement stress evaluation by boundary elements*, Internat. J. Numer. Methods Engrg., 39 (1996), pp. 2399–2415.
[54] Z. Y. Zhao and S. Lan, *Boundary stress calculation—a comparison study*, Comput. & Structures, 71 (1999), pp. 77–85.